Journal of Biomechanics 142 (2022) 111226

Contents lists available at ScienceDirect

Journal of Biomechanics

journal homepage: www.elsevier.com/locate/jbiomech

Finite element analysis of mitral valve annuloplasty in Barlow's disease

Hans Martin Aguilera [a], Stig Urheim [b,c], Robert Matongo Persson [b], Rune Haaverstad [b,c], Bjørn Skallerud [a], Victorien Prot [a,*]

[a] Department of Structural Engineering, Norwegian University of Science and Technology, Trondheim, Norway
[b] Department of Heart Disease, Haukeland University Hospital, Bergen, Norway
[c] Department of Clinical Science, Faculty of Medicine, University of Bergen, Bergen, Norway

ARTICLE INFO

Keywords:
Finite element
Annuloplasty
Mitral valve
Patient specific
Barlow's Disease
Mitral regurgitation

ABSTRACT

Barlow's Disease affects the entire mitral valve apparatus causing mitral regurgitation. Standard annuloplasty procedures lead to an average of 55% annular area reduction of the end diastolic pre-operative annular area in Barlow's diseased valves. Following annular reduction, mitral valvuloplasty may be needed, usually with special focus on the posterior leaflet. An *in silico* pipeline to perform annuloplasty by utilizing the pre- and -postoperative 3D echocardiographic recordings was developed. Our objective was to test the hypothesis that annuloplasty ring sizes based on a percentage (10%–25%) decrease of the pre-operative annular area at end diastole can result in sufficient coaptation area for the selected Barlow's diseased patient. The patient specific mitral valve geometry and finite element model were created from echocardiography recordings. The post-operative echocardiography was used to obtain the artificial ring geometry and displacements, and the motion of the papillary muscles after surgery. These were used as boundary conditions in our annuloplasty finite element analyses. Then, the segmented annuloplasty ring was scaled up to represent a 10%, 20% and 25% reduction of the pre-operative end diastolic annular area and implanted to the end diastolic pre-operative finite element model. The pre-operative contact area decrease was shown to be dependent on the annular dilation at late systole. Constraining the mitral valve from dilating excessively can be sufficient to achieve proper coaptation throughout systole. The finite element analyses show that the selected Barlow's diseased patient may benefit from an annuloplasty ring with moderate annular reduction alone.

1. Introduction

Degenerative mitral valve (MV) diseases is one of the most frequent causes of mitral regurgitation (Iung et al., 2007). Barlow's Disease (BD) affects the entire mitral valve apparatus by altering several fundamental mechanisms characterized by myxomatous infiltration causing leaflet thickening, excessive leaflet tissue, leaflet billowing, severe annular dilation, a diminished annular saddle shape and often, mitral annular disjunction accompanied with multiple regurgitant jets (Hjortnaes et al., 2016; Anyanwu and Adams, 2007; Barber et al., 2001a; Apor et al., 2016).

Mitral valve repair on BD valves is a highly complex procedure involving leaflet resections and/or transpositions, chordal transfers, artificial chordae insertions and the implantation of an annuloplasty ring (Adams and Anyanwu, 2008). The use of large annuloplasty rings to remodel the dilated annulus in BD, has earlier been studied (Adams et al., 2006) and is common practice when performing mitral valve repair on BD valves. Moreover, a recent study (Raanani et al., 2021) showed great long-term results with ring only repair for suitable patients with bileaflet prolapse and no chordae rupture, including BD. During surgery, the annuloplasty rings are commonly sized based on the anterior leaflet size and annuloplasty rings usually range in size from 36–40 mm (commissure-to-commissure distance) in BD mitral valves. The annuloplasty ring sizing is of importance due to the risk of systolic anterior motion, which occurs when the anterior leaflet or excessive tissue is pushed into the left ventricular outflow tract. Mitral annular area of BD mitral valves have been measured to be 15–20 cm^2 in previous studies (Clavel et al., 2015; Sturla et al., 2017), while assuming the annuloplasty ring to be an elliptical shape, ring size 36 and 40 has an area of 7.21 cm^2 and 9.17 cm^2, respectively (Carpentier et al., 2009). The difference between mean annular area of BD mitral valves and the size of commonly used annuloplasty rings to treat this degenerative disease, shows that current annuloplasty rings severely reduce the annular area of BD mitral valves.

In previous years, studies reporting ring annuloplasty simulations on mitral valves with functional mitral regurgitation have been conducted

* Correspondence to: Department of Structural Engineering, Norwegian University of Science and Technology, Richard Birkelands vei 1a, Trondheim, Norway.
E-mail address: victorien.prot@ntnu.no (V. Prot).

https://doi.org/10.1016/j.jbiomech.2022.111226
Accepted 15 July 2022
Available online 25 July 2022

(Stevanella et al., 2011; Choi et al., 2017; Votta et al., 2007; Kong et al., 2018). However, these simulations have limited dynamics in their pre-operative analysis and the mitral annular motion after ring annuloplasty is constrained. In this paper, a patient-specific mitral valve model of a BD mitral valve has been subjected to *in silico* annuloplasty where the displacement boundary conditions for both annulus and papillary muscle tips are extracted from the post-operative (PostOP) echocardiography. The implanted annuloplasty ring has then been scaled based on the pre-operative (PreOP) end-diastolic (ED) area to simulate only moderate reductions in mitral annular area. Combining the Pre- and PostOP echocardiographic assessments creates a robust pipeline to run *in silico* simulations of the annuloplasty procedure with a correct estimate of the annular and papillary muscle (PM) movements. Ring annuloplasty stabilizes the mitral valve dynamics, and with PostOP information we can simulate annuloplasty procedures with a more realistic post-operative movement than prior studies. The present study indicates that annuloplasty based on a moderate downsizing of the mitral annular area may be sufficient to achieve competent valve closure in the selected BD patient as compared to current annuloplasty ring designs.

2. Material and methods

2.1. Patient-specific mitral valve model

The patient included in the present study was a 52-year-old male diagnosed with BD. The patient had bileaflet prolapse with late systolic severe central regurgitation. Furthermore, annular disjunction was detected and no chordal rupture. The studied subject gave written informed consent, and the study protocol was approved by the Regional Committees on Biomedical Research Ethics. The patient-specific Barlow's MV model was created by following the pipeline presented in Aguilera et al. (2021). The FE modeling is summarized below.

The mitral valve leaflets were segmented at ED by analysis of the 3D echocardiographic recordings in the image computing platform 3D Slicer (Fedorov et al., 2012). The annular structure and papillary muscle tips were annotated for all time frames from ED to mitral valve opening (MVO) capturing the dynamic movement of the MV. The generated movement is then implemented into the Abaqus user subroutine VDISP. On the ventricular mitral valve surface, a patient-specific peak pressure was applied following a physiological load amplitude. For the anterior and posterior leaflets, the reduced three noded general-purpose element (S3R) was used, while the chordal structures were modeled as two-noded 3D truss elements (T3D2). Furthermore, the overall leaflet thickness was set to 3 mm which is the average thickness of Barlow leaflets (Hjortnaes et al., 2016). The circular cross-sectional areas for myxomatous marginal and strut chordae were modeled to be 1.6 mm^2 and 2.22 mm^2 respectively (Barber et al., 2001b).

The Gasser–Ogden–Holzapfel (GOH) material model, available in the Abaqus material library (Abaqus, 2014; Gasser et al., 2006), was used with the fitted material parameters of myxomatous degenerative leaflet tissue presented in Aguilera et al. (2021). Briefly, $J = \det \mathbf{F}$ where $\mathbf{F}$ is the deformation gradient, $\bar{I}_1 = J^{-2/3}\mathbf{1} : (\mathbf{F}^T\mathbf{F})$ and $\bar{I}_4 = J^{-2/3}(\mathbf{F}^T\mathbf{F}) : \mathbf{a}_0 \otimes \mathbf{a}_0$, where $\mathbf{a}_0$ is a unit vector denoting the collagen fiber orientation in the undeformed configuration. Thus, the GOH material model is defined as,

$$W(\bar{I}_1, \bar{I}_4, J) = C_{10}(\bar{I}_1 - 3) + \frac{1}{D}\left(\frac{J^2-1}{2} - \ln(J)\right) + \frac{k_1}{2k_2}(\exp\{k_2(\overline{E})^2\} - 1), \quad (1)$$

with,

$$\overline{E} = \kappa(\bar{I}_1 - 3) + (1 - 3\kappa)(\bar{I}_4 - 1), \quad (2)$$

where C_{10}, D, k_1, k_2 and κ are material parameters. D is a material constant that controls compressibility. Due to the high fluid content in soft tissues such as mitral valve tissue, the tissue is assumed to be nearly incompressible (McEvoy et al., 2018), with a leaflet density set to 1000 kg/m^3. D is therefore set to 0, as recommended by the Abaqus documentation (Abaqus, 2014) to model incompressibility. Moreover, the dispersion parameter κ describes the distribution of the fibers. The material parameters used to model the myxomatous material response are presented in Table 1.

Table 1
Material parameters for modeling myxomatous material response for the mitral valve leaflets and chordae. Material parameters acquired from fitting procedures described in Aguilera et al. (2021). (AL)-Anterior Leaflet, (PL)-Posterior Leaflet.

Eqs. (1) and (2)	c_{10} (MPa)	k_1 (MPa)	k_2	κ
AL/PL	0.0010	0.453	14.7	0.316
Eq. (3)	C_{10} (MPa)	$C_{20..40}$ (MPa)	C_{50} (MPa)	
Basal	0.7694	0	26 793	
Marginal	0.05	0	772.8	

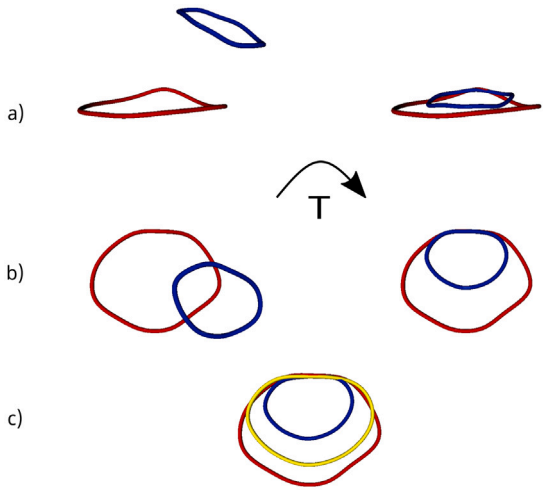

Fig. 1. Transformation from the PostOP (blue) configuration to the PreOP (red) configuration. (a) View looking onto the anterior horn from the posterior side. (b) Surgeons view. (c) Scaling procedure, yellow ring corresponds to 25% reduction in PreOP ED annular area. T is the transformation matrix. (For interpretation of the references to color in this figure legend, the reader is referred to the web version of this article.)

For the myxomatous chordae, a reduced polynomial strain energy function of order 5 was used, with parameters from Table 1. A characteristic feature for Barlow patients is the elongated chordae at systole (Carpentier et al., 2010). It was therefore assumed that there was no pre-tension in the chordae. Furthermore, the myxomatous chordae are more extensible compared to healthy human chordae (Barber et al., 2001b), this is accounted for by implementing myxomatous material parameters for the chordae.

$$\Psi_{Reduced} = \sum_{i=1}^{5} C_{i0}(\bar{I}_1 - 3)^i. \quad (3)$$

The PostOP 3D echocardiography was further used to segment and analyze the PostOP behavior of the mitral valve. Moreover, the PostOP mitral annulus and PM movements were used to supply the *in silico* analyses with a proper annular displacement after annuloplasty. The PostOP analyses were run without any increased stiffness near the sutures after leaflet resections, nor any stiffer chordae mimicking the inserted neochordae, to simulate a post-operative ring only repair approach.

2.2. In silico annuloplasty pipeline and scaling

The *in silico* annuloplasty procedure was performed by utilizing both Pre- and PostOP echocardiographic assessments together with the

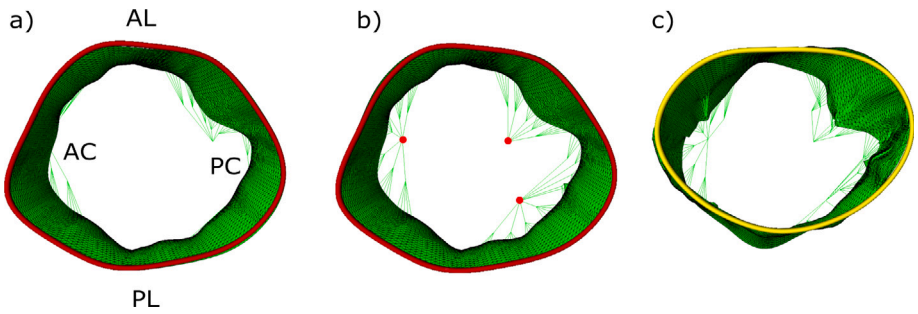

Fig. 2. *In silico* annuloplasty procedure. (a) ED PreOP finite element geometry. Anterior Leaflet (AL), Posterior Leaflet (PL), Anterolateral Commissure (AC), Posteromedial Commissure (PC). (b) The papillary muscle tips are displaced to the PostOP papillary muscle location. (c) The annulus area is reduced by a percentage reduction based on the PreOP ED area. Red line — PreOP ED Annulus. Yellow line −25% reduction annuloplasty ring. (For interpretation of the references to color in this figure legend, the reader is referred to the web version of this article.)

segmented annuloplasty ring and measurements of the Physio Ring II size 36 (Carpentier et al., 2009).

First, the PostOP annulus was annotated from echocardiography for all time frames during the cardiac cycle. Due to small changes in measured PostOP annular area during the cardiac cycle, the implanted annuloplasty ring was assumed to remain stiff with no area change, leaving only a rigid annular motion to be incorporated in the simulation. To determine the rigid body motion, the displacements of the geometric center of the PostOP annulus were used to assign the rigid body translations. For the rotations, we performed a principal component analysis (PCA) of the annulus spline at each time step. The rotation angles of the principal axes obtained from the PCA analysis were used to define the rigid body rotations. The pre- and PostOP echocardiographic assessments do not share the same probe-axis and therefore not the same coordinate systems. Thus, in 3D Slicer the ED configuration of the annuloplasty ring was aligned manually to the anterior horn and the fibrous trigones of the PreOP ED MV (Fig. 1). Between the two configurations, a transformation matrix T was established enabling the transformation of the PostOP coordinate system onto the PreOP coordinate system. T is then used to transform the annotated annuloplasty and papillary muscle movements to the PreOP configuration, enabling the implementation of PostOP dynamics, mimicking an expected stabilized outcome of annuloplasty on the PreOP FE-model. Lastly, the transformed annuloplasty ring is scaled up to represent a percentage decrease in ED PreOP annular area. In the present study, the *in silico* annuloplasty analyses run are based on a 10%, 20% and 25% reduction in PreOP annular area, testing how only moderate annular area reductions affect mitral valve closure. The *in silico* annuloplasty procedure is initiated in the displacement boundary condition VDISP, where first the PM tips are moved linearly to the PostOP location (Fig. 2b). Then, the annular nodes of the PreOP FE geometry are displaced, aligning with the scaled annuloplasty ring (Fig. 2c). To this end, the PreOP and the artificial ring are modeled as periodic degree-3 spline curves parameterized by arc length. Then, the relative parameterization of these annular curves was optimized to find the point-wise map that minimized the total displacement of the procedure as described by Rego et al. (2018). After this initiation step, the PostOp annular and papillary muscle movements, and the ventricular pressure are applied, simulating a scaled rigid annuloplasty ring with PostOP annular and papillary dynamics.

To summarize, a total of five FE analyses are performed: PreOP and PostOP, and three *in silico* analyses with 10%, 20% and 25% annular reduction using the PreOP segmented MV leaflets with PostOP annular and PM dynamics. Note that in the three *in silico* analyses, the MV leaflet area is the same as in the PreOP analysis.

2.3. Analysis

The contact area (CAREA) between the MV leaflets from the finite element analysis is extracted and interpreted as the coaptation area between the mitral valve leaflets. The CAREA was normalized by dividing the CAREA by the total segmented leaflet area from Table 2. The normalized CAREA is used for comparison between the different cases as the total segmented area of the PostOP MV is less than the PreOP one due to leaflet resection. Furthermore, the pre- and PostOP echocardiographic assessment did not have the same frame rate, hence the timescale was also normalized. The annular area was calculated by projecting the annular spline onto its least square plane (LSQ) and calculating the 2D annular area. The longitudinal annular displacement is calculated by computing the scalar product between the ED LSQ-plane normal and the vector between the current and the ED geometric annular center (Fig. 3). The distance from the current annular LSQ-plane and the current PM is calculated for all PMs. Lastly, the maximum in-plane principal stresses and strains were extracted for the PreOP and 25% scaled analysis.

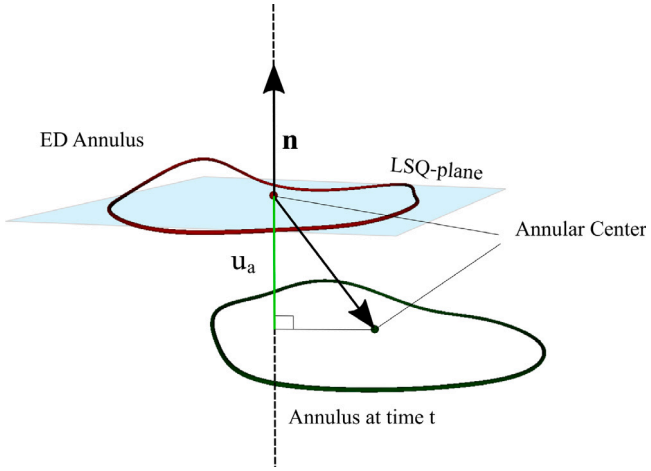

Fig. 3. Longitudinal annular displacement (u_a) calculation based on scalar product between the ED LSQ-plane normal and the vector from ED annular center to the annular center at time t.

3. Results

3.1. Model validation and measurements

The FE model was validated by projecting each node at mitral regurgitation start (MRS) onto the true (imaged) mitral valve geometry as described in Aguilera et al. (2021). At MRS the mitral valve leaflets were segmented based on echocardiography and the distance error between the FE analysis and the segmented surface was calculated. In Fig. 4, an atrial view of the FE meshes and each node's distance to echocardiography is presented. The mean point-to-mesh distance

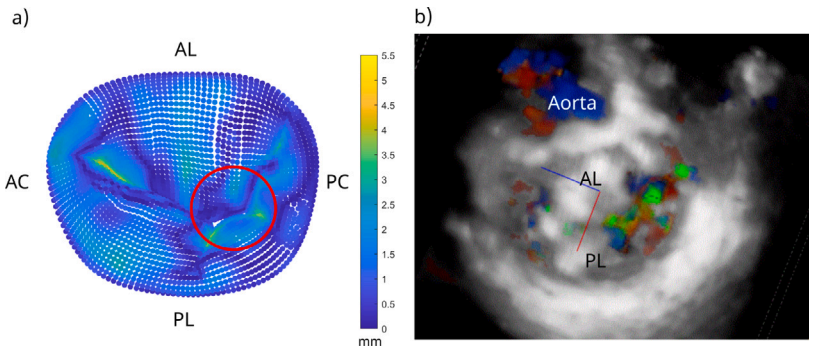

Fig. 4. (a) Atrial view of the point-to-mesh distance error (in mm) between the FE mesh and the true (imaged) configuration at Mitral Regurgitation Start (MRS). The red circle shows where the coaptation defect was observed in the simulation (see also Fig. 8a). (b) Atrial view of late systolic mitral regurgitation in the posteromedial region by 3D echo color Doppler. (For interpretation of the references to color in this figure legend, the reader is referred to the web version of this article.)

Table 2
Patient-specific Pre- and PostOP mitral valve measurements. SLA — Segmented Leaflet Area.

	AL height [mm]	PL height [mm]	SLA [mm^2]
PreOP	31.2	26.3	3031
PostOP	30.2	20.1	2095

was calculated to be 1.63 ± 1.31 mm. A sensitivity analysis was performed on the mesh density, and the mesh that has been used gives convergence in terms of global displacement. In our previous study (Aguilera et al., 2021), several material properties were employed for the mitral valve leaflets, and the myxomatous material parameters were also employed for the patient in the present study. Lastly, the studied patient experienced a closure defect in the posteromedial region as shown in the color Doppler image (Fig. 4b), which coincides with the closure defect observed in the FE model (Fig. 8.)

In Table 2, the Pre- and PostOP mitral valve measurements are presented. The posterior leaflet length is reduced by 6.2 mm in the P2 region post-operatively, which is related to the posterior leaflet length reduction during surgery. Moreover, there is a substantial decrease in segmented leaflet area PostOP. The segmented leaflet area is reduced more than leaflet resected, as the mitral valve leaflets fold during annular reduction, which is difficult to observe on echocardiography. By normalizing the CAREA with the segmented leaflet area, the folding will not affect the results as the folding leaflets, which are not accounted for, are in contact.

3.2. Annular area and papillary muscle to annulus distance

After surgery, the ED annular area is reduced by 61.2% and remains constant throughout the cardiac cycle (Fig. 5a). As shown in 5b, the longitudinal annular displacement of the PostOP mitral annulus moves down towards the left ventricle in systole and returns to its initial position in diastole. For the PreOP annulus, we observe an increase in annular area from ED to late systole of 32.7%. Moreover, pre-operatively the annulus initially moves towards the atrium followed by movement towards the ventricle in systole. At mitral valve opening (MVO), we observe that the longitudinal annular displacement into the ventricle (Fig. 5b) has reduced by 45.8% after surgery.

The papillary muscle tips distance to the LSQ annular planes are calculated pre- and post-operatively (Fig. 5.c) for all time frames throughout the cardiac cycle. It should be noted that there were located two PM tips on the anterolateral PM head pre-operatively, however due to neochordae insertions during surgery, the same PM head post-operatively only had one distinct tip on the echocardiography. Therefore, only one PM was modeled in the anterolateral region PostOP. It is shown that the PreOP PMs moves towards the annular plane from peak systole to MVO, while the PostOP PMs holds a constant distance from the annular plane during the simulation interval.

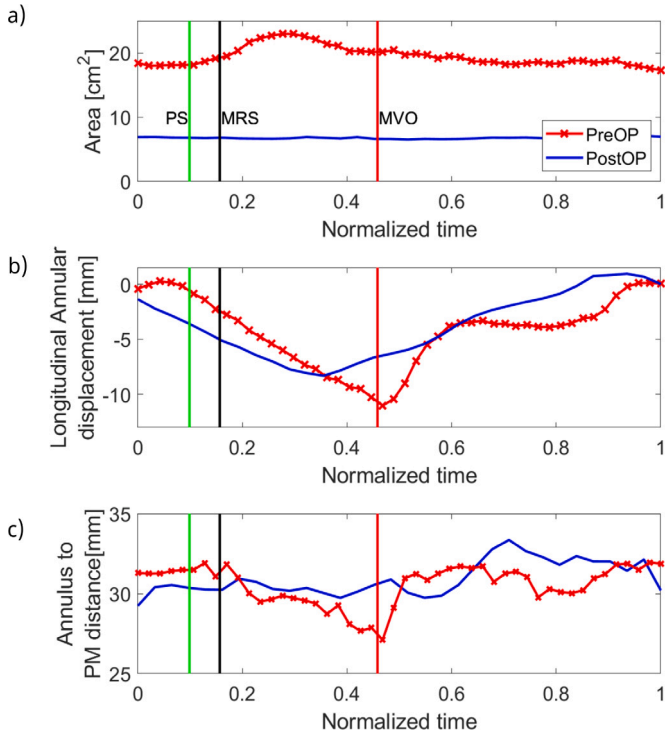

Fig. 5. Pre- and PostOP: (a) Annular area curves. (b) Longitudinal annular displacement. (c) mean PM distance to annular plane. Peak Systole (PS), Mitral Regurgitation Start (MRS), Mitral Valve Opening (MVO).

3.3. Contact area and mitral valve closure

For the PreOP analysis, as shown in Figs. 6a and 7, there is a substantial decrease in CAREA in late systole after MRS. Additionally, coinciding with the onset of CAREA decrease, PreOP annular area begins to dilate (Fig. 5). By differentiating the CAREA and annular area with respect to time, we calculate two late-systolic peaks on the differentiated curves occurring at 0.204 and 0.215 for the CAREA and annular curve, respectively. Furthermore, the initiation of annular dilation and CAREA decrease are observed in Figs. 5 and 7 to coincide with MRS (0.156).

In late systole, the CAREA is shown to be reduced substantially overall in Fig. 6a, with a coaptation height of 2.8 mm in the A2/P2 region where contact is still maintained. For all *in silico* analyses there is shown to be leaflet coaptation for all segments of the mitral valve. The coaptation lengths in the A2/P2 segments are increased for all annuloplasty procedures with peak systolic coaptation lengths from

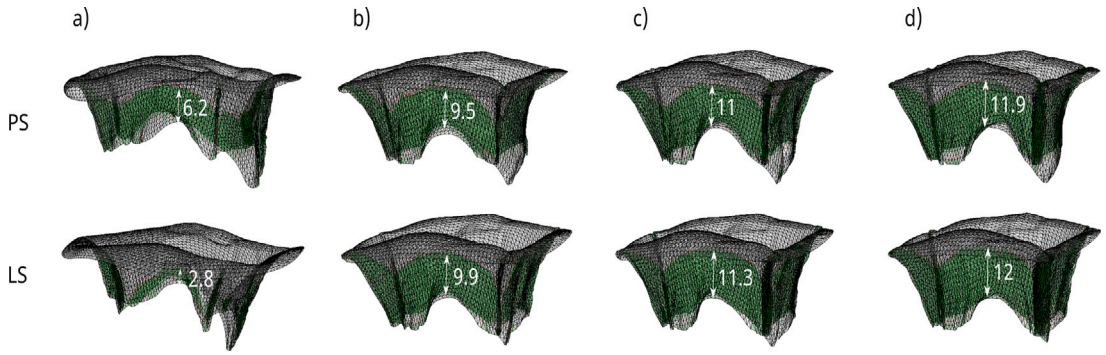

Fig. 6. Coaptation area at Peak Systole (PS) and Late Systole (LS), with coaptation lengths measured in mm on the A2/P2 segments. (a) PreOP. (b) Scaled 10%. (c) Scaled 20%. (d) Scaled 25%.

9.5 mm to 11.9 mm, which is consistent with the findings by Rim et al. (2015).

From Fig. 7a, the normalized CAREA curves for the *in silico* analyses and the PostOP analysis are maintained throughout systole, only affected by the decline in ventricular pressure. Comparing the normalized *in silico* CAREAs with the normalized PostOP CAREA, we observe that a 20% to 25% reduction in PreOP annular area yield CAREAs close to that of the PostOP analysis.

Three additional *in silico* analyses with PreOP rigid annular motion and PM dynamics were run to investigate the influence of these boundary conditions on the annuloplasty procedure. The CAREAs for these simulations are shown in Fig. 7b. As can be seen, the *in silico* analyses show approximately the same CAREA curves as the analyses with the stabilized boundary conditions. However, after MRS the annuloplasty analyses from Fig. 7b, show tendencies to a slight decrease compared to the analyses from Fig. 7a.

In Fig. 8a, the PreOP analysis is shown to have lack of closure at MRS in the P2/P3 region, while all the annuloplasty analyses are shown to stay closed at MRS. Moreover, comparing the annuloplasty analyses with PostOP closure (Fig. 8a), the PostOP analysis has a more symmetrical closure and is substantially smaller following the annular reduction of 61.2% after surgery.

3.4. Stresses and strains

The maximum in-plane principal stresses and strains are extracted at peak systole and plotted on the loaded mitral valves for the PreOP and all *in silico* annuloplasty analyses (Fig. 8b). At peak systole we observe that the maximum in-plane principal stresses and strains are gradually reduced following annular area reduction, especially for the posterior leaflet.

4. Discussion

In the current study, we have developed a pipeline to perform *in silico* annuloplasty by using the post-operative rigid annular motion and PM movement. We have further demonstrated the effect of an annuloplasty ring size based on a percentage decrease in ED mitral annular area pre-operatively, and that by reducing the pre-operative annular area by only 25% versus 61.2% the normalized contact area is approximately the same as the post-operative normalized contact area. Moreover, preventing the annulus from dilating in late systole yields competent valve closure for all scaling procedures (Fig. 8a).

The coaptation defect shown in the FE model (Fig. 8a) was similar to the echocardiographic finding pre-operatively (Fig. 4b). As shown in Fig. 4a, by mean point-to-mesh distance error, the FE model and the echocardiographic image corresponds well. However, near the A3/P3 region, our model exhibits up to 5 mm error. Additionally, our model did not reproduce the bileaflet prolapse, as bileaflet prolapse is defined when a coapting segment over-rides the mitral annular plane

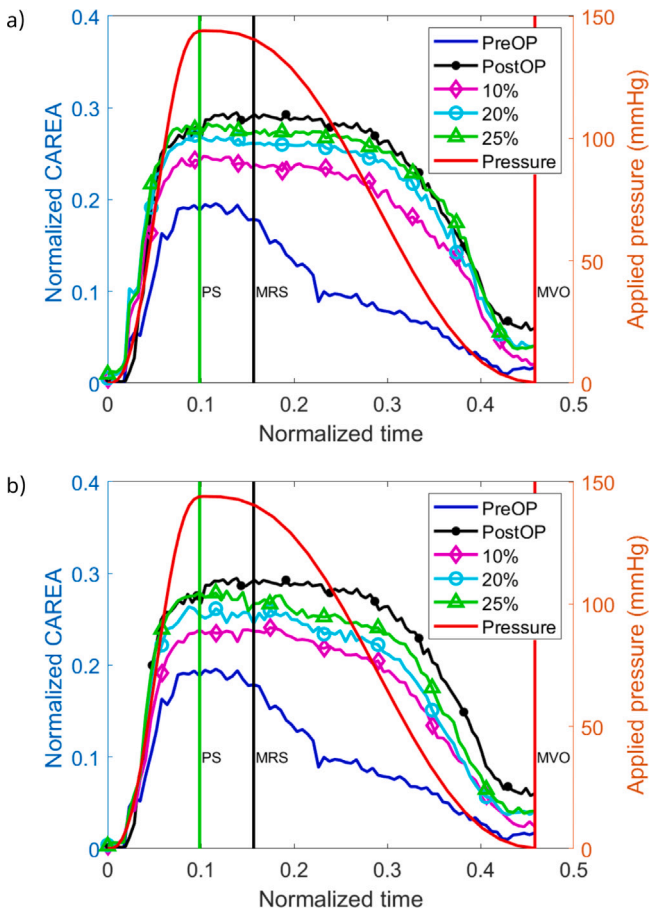

Fig. 7. CAREA normalized with the total segmented leaflet area of PreOP, PostOP, 10%, 20% and 25% scaled annuloplasty from ED to MVO. Annuloplasty simulations with (a) PostOP and (b) PreOP rigid annular motion and PM dynamics.

(Tomši et al., 2017). This may be due to an underestimation of chordal lengthening in this work.

For this patient, we observe that the annulus and papillary muscles motions becomes significantly more stabilized post-operatively during systole as illustrated in Fig. 5b–c. We expect that this stabilization will occur even with larger artificial rings, as these would prevent excessive annular dilation. Yet, it is not possible to predict the exact outcome of such annuloplasty procedures. Therefore, we chose to implement the observed post-operative rigid annular motion and PM dynamics in our *in silico* annuloplasty procedures.

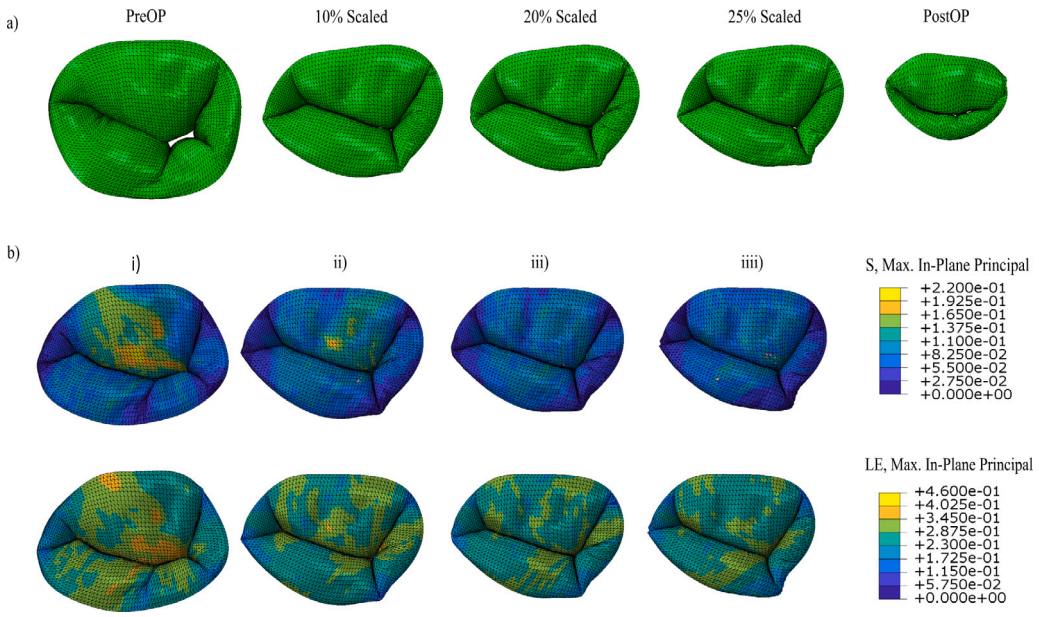

Fig. 8. (a) Mitral valve closure at MRS for the different cases. (b) Maximum in-plane principal stresses (MPa) and logarithmic strains plotted on a surgeons view at peak systole for (i) PreOP, (ii) Scaled 10%, (iii) Scaled 20%, (iv) Scaled 25%. (For interpretation of the references to color in this figure legend, the reader is referred to the web version of this article.)

4.1. Contact area

In our previous paper (Aguilera et al., 2021), we showed that annular dilation is inversely proportional to CAREA decrease for BD mitral valves. The patient studied in the present study shows similar behavior, where the CAREA decrease takes place at approximately the same time as the annular area increase. Measured pre-operatively, MRS occurs at the onset of annular dilation and CAREA reduction, showing that the annular dilation initiates the late systolic alterations in the mitral valve.

To investigate the effects of these boundary conditions on the response of our model, pre-operative boundary conditions (pathological behavior) were also implemented for the three annuloplasty simulations. For these additional simulations, Fig. 7b shows a slight decrease in CAREA after MRS. This may be due to the pre-operative pathological longitudinal annular displacement down into the ventricle. However, these results are still close to those obtained with the post-operative rigid annular motion and PM dynamics (Fig. 7a). In a real-life scenario, we expect the boundary conditions to be close to these two cases. The major contributor to malcoaptation is, for the studied patient, the annular dilation. Therefore, the choice made in this work may not have a great impact on the leaflet coaptation response. Ideally, the dynamics of the annulus and PM for *in silico* simulations would be better obtained by simulating the left ventricle together with the valve. However, very little is known about the mechanics and electrophysiology of the left ventricle in Barlow's disease. Therefore, such an approach would introduce more uncertainties in the simulations at this stage.

Preventing the excessive annular dilation in late systole by *in silico* annuloplasty is shown to eliminate the CAREA decrease, keeping the mitral valve leaflets in apposition through systole. For all *in silico* analyses conducted in this paper, late systolic valve incompetence was prevented. Constraining the MV from dilating excessively can be sufficient to achieve coaptation throughout systole. The *in silico* analyses indicate that the selected BD patient may benefit from an annuloplasty ring with only moderate annular reduction.

Comparing the normalized CAREA curve of the pre- and post-operative analyses we observe that 25% reduction in ED pre-operative annular area yields a normalized CAREA close to the post-operative analysis. For the *in silico* annuloplasty analyses, only the mitral annulus and PM locations were altered without the use of supplementary procedures such as leaflet resection, chordal transpositions and neochordae insertions. Therefore, it was unexpected that the *in silico* analysis and post-operative analysis provided similar functional results, as the valve underwent supplementary procedures during surgery. Thus, the post-operative analysis should only function as a target of how big a fraction of the leaflet that should be in contact to achieve proper closure.

4.2. Annular area and papillary muscle distance from annulus

Comparing the longitudinal annular displacement pre- and post-operatively, the post-operative longitudinal annular displacement is observed to be more predictable, moving only towards the ventricle during systole, while the pre-operative annulus demonstrated a paradoxical initial movement into the atrium followed by a movement towards the left ventricle in systole. At MVO we observe that the pre-operative annulus displaces 45.8% more towards the apex compared to the post-operative annulus. The difference in longitudinal annular displacement clearly shows the need to implement displacement boundary conditions that correspond to the stable post-operative longitudinal annular displacement when performing in-silico annuloplasty procedures. The patient's mitral annular disjunction may also contribute to this abnormal movement, which is stabilized by the annuloplasty ring. In Fig. 5a, there can be observed small variations in the post-operative annular area due to the manual segmentation of the artificial annulus from echocardiography. Thus, since they are very small we have only incorporated the rigid body motion of the post-operative annulus.

From Fig. 5c, the papillary muscles pre- and post-operatively are shown to keep a constant distance from the annular plane from ED to MVO, showing that the papillary muscle movement is controlled by the longitudinal annular displacement in this time interval. Therefore, due to the paradoxical movement of the pre-operative annulus and the papillary muscles, the post-operative papillary muscle information should be used for *in silico* annuloplasty. Post-operatively, the papillary muscle tips can be difficult to distinguish from echocardiographic recordings due to the sonographic shadowing of the neochordae sutures. Therefore, post-operatively, we were not able to separate the two papillary muscle heads anterolaterally. On the other hand, the intensity of the neochordae sutures in the papillary muscles made it easy to find

the papillary muscles on echocardiography. Moreover, in systole when the papillary muscle heads are loaded, they become close together, therefore not being able to distinguish them will not impact the valve closure substantially.

4.3. Stresses and strains

We observe a reduction in maximum in-plane principal stresses and strains on the posterior leaflet after *in silico* annuloplasty (Fig. 8b). Such a reduction in stresses was also reported by Rim et al. (2015), while Ge et al. (2014) only observed reductions in stresses in the anterior leaflet and an increase in stresses on the posterior leaflet. It should be noted that both studies performed annuloplasty and leaflet resections, and not ring only repair as presented in this study. Other computational works on artificial chordal insertions on degenerative mitral valves with posterior leaflet prolapse due to chordal rupture have also shown reduced stresses in the posterior leaflet following repair (Sturla et al., 2014; Rim et al., 2014). During the annuloplasty procedure, the annuloplasty ring is aligned with the anterior horn and trigones which reduces the mitral septal-lateral dimension by displacing the posterior annulus in the septal-lateral direction (see Fig. 2c). As the reduction in mitral annular size mainly affects the posterior side of the annulus, we also observe most stress and strain reductions in the posterior leaflet. With current annuloplasty ring design the posterior leaflet often needs to be resected due to the risk of systolic anterior motion. With a more moderate reduction as shown in this paper, the need for resection in the posterior leaflet may be avoided as both leaflets now contribute to closure.

4.4. Clinical relevance and considerations

The pipeline presented in this study was created to investigate how a moderate annular area reduction would affect mitral valve closure during ventricular systole. For Barlow's diseased mitral valves experiencing late systolic regurgitation without prolapse due to chordal rupture, inserting a patient-specific annuloplasty ring based on a percentage reduction of the pre-operative end diastolic annular area may result in successful repair without the need for additional mitral valvuloplasty. Repair of a mitral valve diagnosed with Barlow's disease is commonly a highly complex procedure due to the need for varying individualized repair techniques. We speculate that several of these techniques are used due to too severe annular reduction, therefore only moderate reductions and prevention of late systolic annular dilation may be sufficient. However, Barlow's disease is a dynamic degenerative process and though being able to accurately reproduce the immediate post-operative outcome, we may not be capable to predict the long-term outcome. In recent studies (Raanani et al., 2021), Barlow's mitral valves have been repaired with rings only in selected patients, simplifying the complexity of the repair strategy. However, choosing the correct ring is often a challenge and the study presented herein can help optimize the ring size and shape for each individual patient. Only one patient is included in the present work. Therefore, further studies need to be conducted on several patients with similar etiology to get a better understanding of the benefit of such an annuloplasty procedure. The present paper introduces the pipeline to further study this.

CRediT authorship contribution statement

Hans Martin Aguilera: Writing – original draft, Visualization, Software, Methodology, Investigation, Formal analysis, Conceptualization. **Stig Urheim:** Writing – review & editing, Visualization, Supervision, Resources, Methodology, Investigation, Funding acquisition, Conceptualization. **Robert Matongo Persson:** Writing – review & editing, Methodology, Investigation, Conceptualization. **Rune Haaverstad:** Writing – review & editing, Resources, Investigation. **Bjørn Skallerud:** Writing – review & editing, Supervision, Resources, Methodology, Conceptualization. **Victorien Prot:** Writing – review & editing, Visualization, Supervision, Software, Methodology, Investigation, Funding acquisition, Conceptualization.

Declaration of competing interest

The authors declare that they have no known competing financial interests or personal relationships that could have appeared to influence the work reported in this paper.

Acknowledgments

This document is the results of the research project funded by the Trond Mohn Foundation (TMS2019TMT09).

References

Abaqus, 2014. Abaqus analysis user's guide. Dassault systemes.

Adams, D.H., Anyanwu, A.C., 2008. Seeking a higher standard for degenerative mitral valve repair: begin with etiology. Thorac. Cardiovasc. Surg. 3 (136), 551–556.

Adams, D.H., Anyanwu, A.C., Rahmanian, P.B., Abascal, V., Salzberg, S.P., Filsoufi, F., 2006. Large annuloplasty rings facilitate mitral valve repair in Barlow's disease. Ann. Thorac. Surg. (ISSN: 00034975) 82 (6), 2096–2101. http://dx.doi.org/10.1016/j.athoracsur.2006.06.043.

Aguilera, H., Urheim, S., Skallerud, B., Prot, V., 2021. Influence of annular dynamics and material behavior in finite element analysis of Barlow's Mitral valve disease. J. Elasticity (145), 163–190. http://dx.doi.org/10.1007/s10659-021-09829-5.

Anyanwu, A.C., Adams, D.H., 2007. Etiologic classification of degenerative mitral valve disease: Barlow's disease and fibroelastic deficiency. Semin. Thorac. Cardiovasc. Surg. 19 (2), 90–96. http://dx.doi.org/10.1053/j.semtcvs.2007.04.002.

Apor, A., Nagy, A.I., Kovács, A., Manouras, A., Andrássy, P., Merkely, B., 2016. Three-dimensional dynamic morphology of the mitral valve in different forms of mitral valve prolapse - Potential implications for annuloplasty ring selection. Cardiovasc. Ultrasound 14 (1), http://dx.doi.org/10.1186/s12947-016-0073-4.

Barber, J.E., Kasper, F.K., Ratliff, N.B., Cosgrove, D.M., Griffin, B.P., Vesely, I., 2001a. Mechanical properties of myxomatous mitral valves. J. Thorac. Cardiocasv. Surg. 122 (5), 955–962. http://dx.doi.org/10.1067/mtc.2001.117621.

Barber, J.E., Ratliff, N.B., Cosgrove 3rd, D.M., Griffin, B.P., Vesely, I., 2001b. Myxomatous mitral valve chordae. I: Mechanical properties. 2001/05/31 J. Heart Valve Dis. 10 (3), 320–324.

Carpentier, A., Adams, D., Adzich, V., 2009. Mitral valve patient-specific finite element modeling from cardiac MRI: Application to an annuloplasty procedure.

Carpentier, A., Adams, D., Filsoufi, F., 2010. Carpentier's Reconstructive Valve Surgery : From Valve Analysis to Valve Reconstruction, Vol. I. Saunders Elsevier.

Choi, A., McPherson, D.D., Kim, H., 2017. Computational virtual evaluation of the effect of annuloplasty ring shape. Int. J. Numer. Methods Biomed. Eng. 33 (6), e2831. http://dx.doi.org/10.1002/CNM.2831.

Clavel, M., Mantovani, F., Malouf, J., Michelena, H.I., Vatury, O., Jain, M.S., Mankad, S.V., Suri, R.M., Enriquez-Sarano, M., 2015. Dynamic phenotypes of degenerative myxomatous mitral valve disease: quantitative 3-dimensional echocardiographic study. Circ. Cardiovasc. Imaging. 8 (5), http://dx.doi.org/10.1161/CIRCIMAGING.114.002989.

Fedorov, A., Beichel, R., Kalpathy-Cramer, J., Finet, J., Fillion-Robin, J.-C., Pujol, S., Bauer, C., Jennings, D., Fennessy, F.M., Sonka, M., Buatti, J., Aylward, S.R., Miller, J., Pieper, S., Kikinis, R., 2012. 3D slicer as an image computing platform for the quantitative imaging network. Magn. Reson. Imaging 9 (30), 1323–1341.

Gasser, T.C., Ogden, R.W., Holzapfel, G.A., 2006. Hyperelastic modelling of arterial layers with distributed collagen fibre orientations. J. R. Soc. Interface 3 (6), 15–35.

Ge, L., Morrel, W.G., Ward, A., Mishra, R., Zhang, Z., Guccione, J.M., Grossi, E.A., Ratcliffe, M.B., 2014. Measurement of mitral leaflet and annular geometry and stress after repair of posterior leaflet prolapse: Virtual repair using a patient-specific finite element simulation. Ann. Thorac. Surg. (ISSN: 15526259) 97 (5), 1496–1503. http://dx.doi.org/10.1016/j.athoracsur.2013.12.036.

Hjortnaes, J., Keegan, J., Bruneval, P., Schwartz, E., Schoen, F.J., Carpentier, A., Levine, R.A., Hagège, A., Aikawa, E., 2016. Comparative histopathological analysis of mitral valves in Barlow disease and fibroelastic deficiency. Semin. Thorac. Cardiovasc. Surg. (ISSN: 15329488) 28 (4), 757–767. http://dx.doi.org/10.1053/j.semtcvs.2016.08.015.

Iung, B., Baron, G., Tornos, P., Gohlke-Bärwolf, C., Butchart, E.G., Vahanian, A., 2007. Curr. Probl. Cardiol. 32 (11), 609–661. http://dx.doi.org/10.1016/j.cpcardiol.2007.07.002, Current Problems in Cardiology.

Kong, F., Pham, T., Martin, C., Elefteriades, J., McKay, R., Primiano, C., Sun, W., 2018. Finite element analysis of annuloplasty and papillary muscle relocation on a patient-specific mitral regurgitation model. PLoS One (ISSN: 19326203) 13 (6), 1–15. http://dx.doi.org/10.1371/journal.pone.0198331,

McEvoy, E., Holzapfel, G.A., McGarry, P., 2018. Compressibility and anisotropy of the ventricular myocardium: Experimental analysis and microstructural modeling. J. Biomech. Eng. (ISSN: 15288951) 140 (8), 1–10. http://dx.doi.org/10.1115/1.4039947.

Raanani, E., Schwammenthal, E., Moshkovitz, Y., Cohen, H., Kogan, A., Peled, Y., Sternik, L., Ram, E., 2021. Repair with annuloplasty only of balanced bileaflet mitral valve prolapse with severe regurgitation. Eur. J. Cardiothorac. Surg. (ISSN: 1010-7940) http://dx.doi.org/10.1093/ejcts/ezab548.

Rego, B.V., Khalighi, A.H., Drach, A., Lai, E.K., Pouch, A.M., Gorman, R.C., Gorman, J.H., Sacks, M.S., 2018. A noninvasive method for the determination of in vivo mitral valve leaflet strains. J. Numer. Method. Biomed. Eng. 34 (12), http://dx.doi.org/10.1002/cnm.3142.

Rim, Y., Choi, A., McPherson, D.D., Kim, H., 2015. Personalized computational modeling of mitral valve prolapse: Virtual leaflet resection. PLoS One 10 (6), e0130906. http://dx.doi.org/10.1371/JOURNAL.PONE.0130906.

Rim, Y., Laing, S.T., McPherson, D.D., Kim, H., 2014. Mitral valve repair using ePTFE sutures for ruptured mitral chordae tendineae: A computational simulation study. Ann. Biomed. Eng. 42 (1), 139–148. http://dx.doi.org/10.1007/S10439-013-0908-1.

Stevanella, M., Maffessanti, F., Conti, C.A., Votta, E., Arnoldi, A., Lombardi, M., Parodi, O., Caiani, E.G., Redaelli, A., 2011. Mitral valve patient-specific finite element modeling from cardiac MRI: Application to an annuloplasty procedure. Cardiovasc. Eng. Technol. 2 (2), 66–76. http://dx.doi.org/10.1007/s13239-010-0032-4.

Sturla, F., Onorati, F., Puppini, G., Pappalardo, O.A., Selmi, M., Votta, E., Faggian, G., Redaelli, A., 2017. Dynamic and quantitative evaluation of degenerative mitral valve disease: A dedicated framework based on cardiac magnetic resonance imaging. J. Thorac. Dis. 9 (4), S225–S238. http://dx.doi.org/10.21037/jtd.2017.03.84.

Sturla, F., Onorati, F., Votta, E., Pechlivanidis, K., Stevanella, M., Milano, A.D., Puppini, G., Mazzucco, A., Redaelli, A., Faggian, G., 2014. Is it possible to assess the best mitral valve repair in the individual patient? Preliminary results of a finite element study from magnetic resonance imaging data. J. Thorac. Cardiovasc. Surg. 148 (3), 1025–1034. http://dx.doi.org/10.1016/J.JTCVS.2014.05.071.

Tomši, A., Hiemstra, Y.L., Bissessar, D.D., van Brakel, T.J., Versteegh, M.I.M., Ajmone Marsan, N., Klautz, R.J.M., Palmen, M., 2017. Mitral valve repair in barlow's disease with bileaflet prolapse: the effect of annular stabilization on functional mitral valve leaflet prolapse. Interact. Cardiovasc. Thorac. Surg. 26 (4), 559–565. http://dx.doi.org/10.1093/icvts/ivx366.

Votta, E., Maisano, F., Bolling, S.F., Alfieri, O., Montevecchi, F.M., Redaelli, A., 2007. The geoform disease-specific annuloplasty system: A finite element study. Ann. Thorac. Surg. 84 (1), 92–101. http://dx.doi.org/10.1016/j.athoracsur.2007.03.040.